Thin Solid Films 520 (2011) 144–151

Structure and chemical bonds in reactively sputtered black Ti–C–N–O thin films

J.M. Chappé [a], M.C. Marco de Lucas [b,*], L. Cunha [a], C. Moura [c], J.F. Pierson [d], L. Imhoff [b], O. Heintz [b], V. Potin [b], S. Bourgeois [b], F. Vaz [a]

[a] Centro de Física, Universidade do Minho, 4710-057 Braga, Portugal
[b] Laboratoire Interdisciplinaire Carnot de Bourgogne (ICB), UMR 5209 CNRS-Université de Bourgogne, 9 Av. A. Savary, BP 47870, 21078 Dijon Cedex, France
[c] Universidade do Minho, Dept. Física, Campus de Gualtar, 4710-057 Braga, Portugal
[d] Institut Jean Lamour (UMR CNRS 7198), Département CP2S, Ecole des Mines, Parc de Saurupt, CS 14234, 54042 Nancy Cedex, France

Abstract

The evolution of the nanoscale structure and the chemical bonds formed in Ti–C–N–O films grown by reactive sputtering were studied as a function of the composition of the reactive atmosphere by increasing the partial pressure of an O2+N2 gas mixture from 0 up to 0.4 Pa, while that of acetylene (carbon source) was constant. The amorphisation of the films observed by transmission electron microscopy was confirmed by micro-Raman spectroscopy, but it was not the only effect associated to the increase of the O2+N2 partial pressure. The chemical environment of titanium and carbon, analysed by X-ray photoemission spectroscopy, also changes due to the higher affinity of Ti towards oxygen and nitrogen than to carbon. This gives rise to the appearance of amorphous carbon coexisting with poorly crystallized titanium oxynitride. The evolution of the films colour is explained on the basis of these structural changes.

1. Introduction

Nowadays, titanium nitride (TiN) is one of the most important technological coating materials because of its good chemical stability and excellent tribological properties. It is certainly, the most explored hard thin film material and most extensively used in industry. It is used in a wide range of applications, from protective material for machine parts and cutting tools [1] to diffusion barriers in semiconductor technology [2–4].

Beyond its nitride form, titanium is extensively used in several types of carbides. In fact, titanium carbide (TiC) thin films have also found wide application in various tribological engineering devices owing to its excellent hardness associated with an excellent wear resistance [5]. Due to the interesting combination of properties exhibited by both nitride and carbide forms, "mixed" titanium carbonitride thin films, Ti(C,N), have been used in a wide variety of mechanical-based applications, generally to improve tool life [6]. The insertion of carbon increases the resistivity of titanium nitride films, which is detrimental for applications as diffusion barriers. On the other hand, the growth of amorphous carbon can reduce diffusion through grain boundaries [3,4]. Significant amounts of oxygen have usually been found in this kind of films [4,7,8] due to the high affinity of titanium towards oxygen. The insertion of oxygen, as that of carbon, is detrimental for the resistivity of titanium nitride films.

* Corresponding author.
E-mail address: delucas@u-bourgogne.fr (M.C. Marco de Lucas).

In fact, tailoring the amount of oxygen in nitride or carbide materials, one can expect obtaining a wide range of properties, going from metallic carbide/nitrides to an insulating-like behaviour characteristic of oxide-type compounds [9]. As a result, one can expect to obtain a relatively large window of possibilities in terms of electrical and electronic properties, as well as those related with optical features [10]. The materials colour would be one of such optical properties that can be expected to be varied.

So far, few works have been published on the fabrication of quaternary metal oxycarbonitride thin films by controlling the amount of the three non metals. In the particular case of Ti–C–O–N thin films, they have been mainly focused on their tribological properties [11–14]. Moreover, this kind of coatings should also find applications for decorative purposes. In this field it is of high interest to obtain coatings having a large range of possible colours, including the black one, using a simple deposition method. In particular the presence of different targets should not be necessary allowing deposition from a single source. Linked to that it was shown that controlling reaction atmosphere allows varying the composition of titanium oxynitride films formed by laser treatment of a titanium plate [15]. In addition, concerning deposition techniques, magnetron sputtering is a widely used technique for the growth of titanium compounds thin films having a given crystallography: this occurs through the control of different growth parameters such as working pressure [16–18].

So, in a previous work [19], we reported the fabrication of titanium oxycarbonitride films on silicon substrates by direct current reactive magnetron sputtering of a titanium target, while acetylene and a mixture of oxygen and nitrogen were injected into the deposition

chamber. The optical properties of the films varied with the $O_2 + N_2$ partial pressure used in the deposition process. In particular, we showed that the metallic dark grey colour of titanium carbide films becomes deep black with the increase of oxygen and nitrogen amount in the films. X-ray diffraction (XRD) experiments showed the progressive amorphisation of the films structure with the increase of the $O_2 + N_2$ gas pressure. However the evolution of the films colour should not be explained considering only this effect.

In the present work, we analyse in detail the changes in the structure and the chemical bonds of Ti–C–N–O thin films as a function of the gas mixture ($O_2 + N_2$) partial pressure with the aim of explaining the variation of their optical properties and colour. Transmission electron microscopy (TEM), X-ray photoelectron spectroscopy (XPS) and micro-Raman spectroscopy were used for analyzing the films. The growth of amorphous carbon in addition to titanium oxynitride appears as the key to explain the black colour of the films obtained with a high $O_2 + N_2$ partial pressure.

2. Experimental details

The depositions of titanium oxycarbonitride thin films were performed in a laboratory-size unbalanced (type II) direct current (DC) magnetron sputtering system. Experimental details are given in Ref. [19]. The titanium target (purity 99.96%) was sputtered in an argon (working gas) + gas mixture (oxygen and nitrogen source, with a constant O_2:N_2 ratio of 3:17) + acetylene (carbon source) atmosphere. The argon flow and the acetylene flow were kept constant at 60 sccm and 5 sccm, which corresponded to partial pressures of 0.47 Pa and 0.25 Pa, respectively. The gas mixture partial pressure, p_{O2+N2}, was systematically changed from 0 to 0.4 Pa by controlling the gas mixture flow rate (from 0 to 18 sccm). The base pressure was below 10^{-3} Pa.

The evolution of the elemental composition of the deposited films was determined by Electron Probe Micro Analysis. The results (Fig. 1) revealed two domains separated by a small transition zone [19]:

- zone I ($0 < p_{O2+N2} < 0.11$ Pa), where the increase of p_{O2+N2} leads to a decrease of titanium and carbon concentrations, while those of oxygen and nitrogen increase;
- zone II (0.15 Pa $< p_{O2+N2} < 0.40$ Pa), where the increase of p_{O2+N2} leads to the increase of the oxygen concentration, while that of carbon decreases. The concentration of titanium and nitrogen are almost constant.

The film's colour was analysed by using a commercial Minolta CM-2600 d portable spectrophotometer (wavelength range: 400–700 nm), with diffused illumination (D65 light source) at an 8° viewing angle (specular component included). It was equipped with a 52 mm diameter integrating sphere and 3 pulsed xenon lamps. The observer was placed at a 10° angle. Results are represented in the CIELab 1976 colour space.

XRD experiments were performed in a Siemens D-500 apparatus using a Co Kα radiation ($\lambda = 0.178897$ nm) in Bragg-Brentano configuration.

XPS measurements were performed with a SIA 100 Riber system equipped with a 200 W Al K_{alpha} X-ray source (accelerating voltage of 20 kV and emission current of 10 mA) and a Riber MAC 2 spectrometer. The total resolution (Ag 3 $d_{5/2}$ width) was 2.0 eV for survey scans and 1.3 eV for selected spectral windows. Argon ion sputtering with 4 kV accelerating voltage and 20 mA current was applied in order to remove the contamination layer. Carbon component corresponding to C–C and C–H bonds in the C 1s line was used as a reference for spectra binding energy calibration at 284.5 eV. The analysis chamber residual pressure was maintained below 10^{-7} Pa during measurements. Data were treated using the Casa software package.

The samples were also studied by TEM. Cross-sectional samples for TEM were prepared using the standard sandwich technique. They were mechanically polished, dimpled down to a thickness of 10 μm and Ar^+-ion milled to electron transparency. TEM observations were carried out with a 200 kV JEOL 2100 (LaB_6) microscope with a Scherzer resolution of 0.25 nm. The images were recorded with an on-line charged coupled device (CCD) camera and the analyses of the results were performed using the Digital Micrograph software.

Micro-Raman measurements were performed using a Jobin-Yvon T64000 spectrometer equipped with a three stage monochromator working in double subtractive configuration. A nitrogen-cooled CCD was used as detector. The spectra were obtained in back-scattering

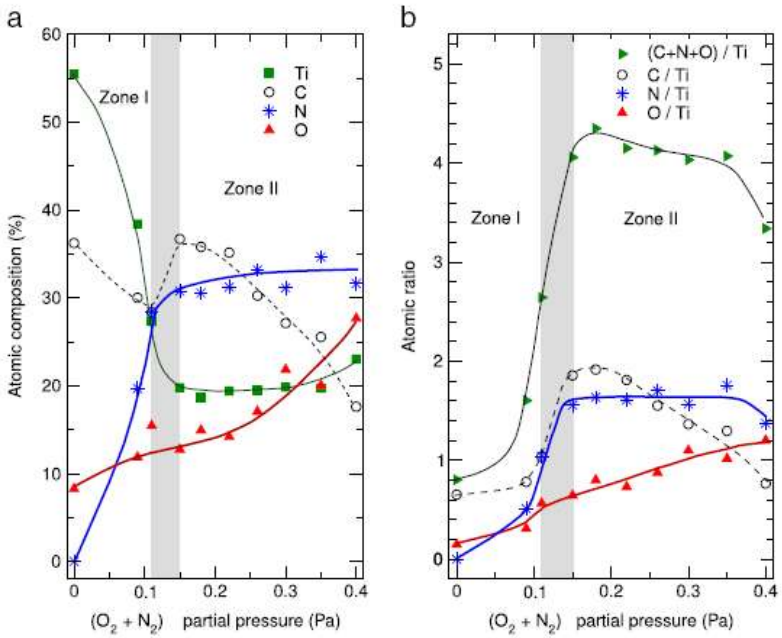

Fig. 1. (a) Evolution of the atomic composition and (b) ratio of non metallic elements (carbon, nitrogen and oxygen) to Ti concentrations as a function of the $O_2 + N_2$ partial pressure.

configuration. An Ar–Kr laser was used as the excitation source. The laser power focused on the sample was kept around 0.4 mW in order to prevent local heating. The spectra shown here were obtained with the laser line at 458 nm.

3. Results

3.1. Structural analysis: TEM and micro-Raman spectroscopy

TEM was used to go further in the structural study of the films previously characterized by XRD [19]. Two representative samples of zones I and II (Figs. 1 and 2) were analysed. The sample corresponding to zone I was deposited with a gas mixture partial pressure of $p_{O2+N2} = 0.09$ Pa. XRD patterns (Fig. 3) showed in this case a face centered cubic (f.c.c.) phase similar to that of TiC obtained for $p_{O2+N2} = 0$. It is worth to note that TiC, TiN and TiO have the same crystallographic structure with close lattice parameters ($a_{TiC} = 0.4328$ nm (JCPDS04-004-2919), $a_{TiN} = 0.4241$ nm (JCPDS04-001-2272) and $a_{TiO} = 0.4177$ nm (JCPDS04-001-6834)). The sample corresponding to zone II was prepared using a partial pressure $p_{O2+N2} = 0.40$ Pa. The absence of peaks in the XRD pattern showed the amorphisation of the films in zone II.

For both samples, a silicon oxide interlayer is observed by TEM, between the silicon substrate and the deposited films, with a thickness of approximately 4 nm (Fig. 4), which is the result of some native surface oxidation of the substrates.

Selected area electron diffraction experiments were also performed for both samples. The comparison of the obtained patterns (Fig. 5a and c) indicates that sample I is more crystallized than sample II, which is in good agreement with XRD results. Sample II appears to be mainly amorphous whereas sample I is mainly polycrystalline. As the grain size is smaller than the selection area used diaphragm, the pattern displays the contribution of several grains with different orientations. It is characterized by the presence of rings whose radii correspond to interreticular distances. The analysis of these patterns using the Bragg's law allowed determining the experimental distances for sample I as equal to $d = 0.247 \pm 0.002$ nm and $d = 0.212 \pm 0.002$ nm.

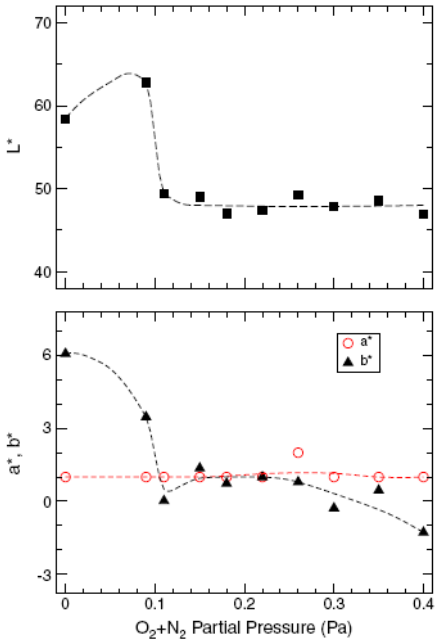

Fig. 2. Average colour coordinates (L*, a*, b*) of Ti–C–O–N films on silicon in the CIELab colour space under the standard CIE illuminant D65, as a function of the $O_2 + N_2$ partial pressure.

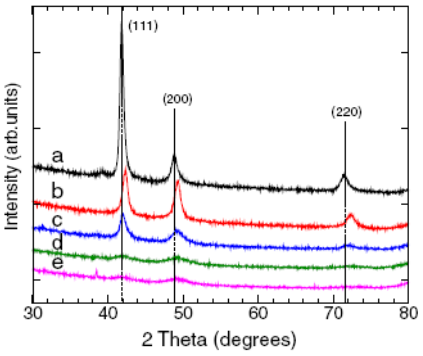

Fig. 3. X-ray diffraction patterns of the films deposited on silicon (100) substrates as a function of the $O_2 + N_2$ partial pressure, from (a) to (e): 0, 0.09, 0.11, 0.15 and 0.18 Pa. Vertical lines correspond to the TiC diffraction peak positions. The patterns were vertically shifted for the sake of clarity.

Dark field images have been obtained by selecting a part of the rings in the diffraction plane with a diaphragm (Fig. 5b and d). The comparison of the density of bright grains in the two images confirms that sample I is more crystallized than the other one. The size of the crystallites was directly measured on the dark field images. Most crystallites are in the 5–10 nm size range, but some of them can be as big as 30 nm. The results are comparable for both samples. They are in agreement with those reported in Ref. [4] for Ti(C,N) films described as amorphous films where some nanocrystallites are embedded.

In order to acquire some more detailed information, observations in high resolution mode (HRTEM) were also carried out, which confirmed the values of particles size mentioned above. Moreover, observation of Moiré fringes in sample I images indicates the presence of superposed crystallized grains with different orientations. For sample II, a few crystallites were also observed and analyzed. Fast Fourier Transformation (FFT) has been applied to HRTEM images of small crystallites. At first, for each pattern, the calibration of the interplanar distances d_{hkl} had to be carried out by studying the FFT of the silicon substrate image. From FFT patterns and after calibration, the experimental d_{hkl} values have been calculated and were found equal to 0.212 ± 0.002 nm and to 0.247 ± 0.002 nm in both samples. This is consistent with the values that were already mentioned from the diffraction patterns analysis of sample I.

The experimental interplanar distances have been compared to the theoretical ones for the anatase and rutile phases of TiO_2, the graphite and diamond phases of carbon and the face-centered cubic phases of TiO, TiN and TiC. This comparison allows eliminating TiO_2 and carbon phases as some theoretical distances are not observed experimentally. As the interplanar distances are relatively close for the three fcc phases ($d_{111} = 0.241$ nm for TiO, 0.245 nm for TiN and 0.250 nm for TiC), it is not possible to identify, without ambiguity, the crystallographic structure of the grains. The overall set of results obtained by TEM is consistent with a nanocrystalline nature of the films where the developed structures are somewhat a mixture of binary ones (carbide-, nitride- and/or oxide-based ones).

In order to have further insights in these structural features, the as-deposited films were studied by micro-Raman spectroscopy. Fig. 6 displays the variation of Raman spectra as a function of the $O_2 + N_2$ partial pressure. For clarity purposes, each spectrum was normalized to the Raman signal at 1580 cm^{-1}. Two spectral regions are shown:

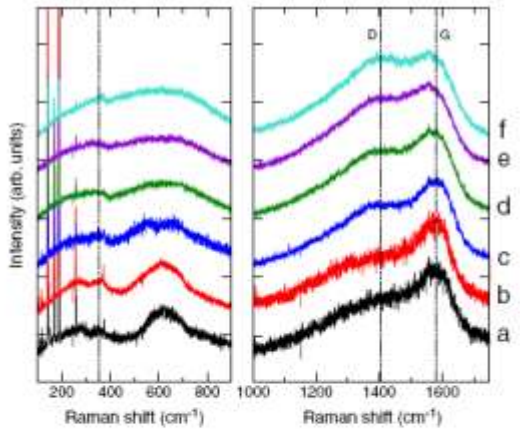

Fig. 6. Raman spectra as a function of the $O_2 + N_2$ partial pressure, from (a) to (f): 0, 0.09, 0.11, 0.15, 0.22 and 0.40 Pa. The spectra were normalized to the Raman intensity at 1580 cm^{-1} and vertically shifted for clarity. Sharp peaks in the very low frequency range (<400 cm^{-1}) are due to the laser plasma lines.

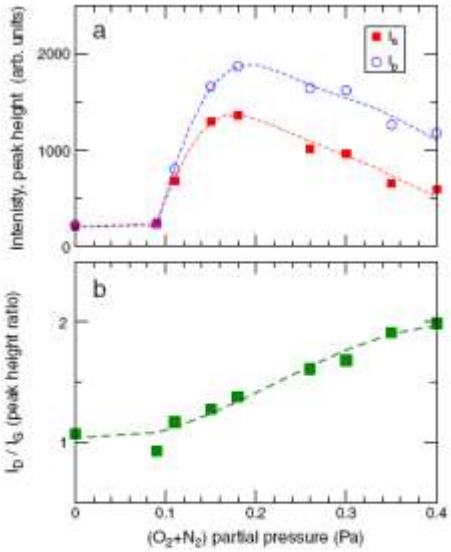

Fig. 7. (a) Intensity (peak height) of G and D Raman bands (C–C stretching modes) as a function of the $O_2 + N_2$ partial pressure. The experimental spectra were fitted by two Gaussians and a straight baseline. (b) I_D/I_G peak height ratio.

respectively, which are characteristic of C–C stretching modes [22–24]. In carbon materials, the G band is due to bond stretching modes (zone center modes of E_g symmetry) of all pairs of sp^2 atoms in both rings and chains. The D band is a breathing mode of A_{1g} symmetry involving phonons near the K zone boundary. This mode is forbidden in the perfect graphite and only becomes active in the presence of disorder. It is due to breathing modes of sp^2 atoms only in rings. The G and D peaks are only due to sp^2 sites. For visible excitation, the cross-section of the sp^2 phase can be up to 250 times that of the sp^3 phase, as visible photons preferentially excite their π states. Thus the sp^2 sites dominate the spectra which depend directly on the configuration of the sp^2 phase [22–24].

The experimental spectra were fitted by two Gaussians and a straight baseline. The intensity (peak height) of D and G-bands is shown in Fig. 7a as a function of the $O_2 + N_2$ partial pressure.

The first result to be noted is the fact of detecting C–C Raman bands even for the film deposited without gas mixture flow ($p_{O2+N2} = 0$ Pa). This means that a fraction of the carbon atoms within the film displays a network out of the TiC phase [21,22]. The intensity of C–C bands is very low for samples in zone I, but it increases strongly for $p_{O2+N2} > 0.1$ Pa (Fig. 7a). This suggests that the fraction of carbon atoms forming the C–C network is very small in zone I, whereas it is high in samples of zone II. This assumption must, however, be taken with care because the probed depth in Raman experiments can vary from one sample to another due to the influence of the composition and the structure on the optical properties of the films.

The position of G and D-bands is almost constant independently of the p_{O2+N2} value. The position of the G-band, 1580 cm^{-1}, is relatively high compared to the usual value in amorphous carbon (a-C). According to Ferrari et al. [22–24], this can be explained as due to the appearance of clustering, which introduces some degree of order inside the amorphous carbon phase. The increase of the clustering process would lead finally to the growth of nanocrystalline graphite (nc-graphite). The full width at half maximum of the G-band, FWHM (G) = 110 cm^{-1}, which is known to increase with structural disorder [22], is consistent with the presence of some order inside an amorphous carbon matrix. The D-band is placed at about 1406 cm^{-1} and its bandwidth decreases slightly from 400 cm^{-1} to 350 cm^{-1} in the transition zone.

Fig. 7b displays the variation of the intensity ratio (peak height ratio) between D and G bands as a function of p_{O2+N2}. The intensity ratio is around 1 in zone I, but it increases up to $I_D/I_G \sim 2$ in zone II. As indicated previously, the D-mode, which is forbidden in the perfect graphite, becomes active in the presence of disorder. Thus, the increase of I_D/I_G in zone II suggests the increase of disorder within the C–C network. With all these results, Raman spectra in the D–G bands range can be assigned to amorphous carbon (a-C) [23,25,26].

3.2. Bonding characteristics: X-ray photoelectron spectroscopy

XPS experiments were carried out for analysing changes in the chemical state and bonds formed by the different elements inside these films. Particular attention was given to the analysis of carbon bands taken into account Raman results. For that, a set of five samples was chosen, two from zone I ($p_{O2+N2} = 0$ and 0.09 Pa), two from zone II ($p_{O2+N2} = 0.22$ and 0.40 Pa) and one corresponding to a transition state between zones I and II ($p_{O2+N2} = 0.11$ Pa). The (C + N + O)/Ti atomic ratios (Fig. 1) corresponding to the selected samples are 0.8 and 1.6 in zone I, 3.3 and 4.1 in zone II, and 2.6 in the transition zone.

The evolution of the Ti 2p line as a function of the gas mixture partial pressure is presented in Fig. 8. In a general point of view, decomposition of such a line in elementary contributions is especially hazardous by the fact that nitrogen, oxygen and carbon can be linked to titanium, as previously inferred from the composition analysis. In spite of this difficulty, several results were obtained.

In the case of the lowest $O_2 + N_2$ partial pressures (zone I), corresponding also to the lowest O/Ti, N/Ti and C/Ti ratios, the shape of the Ti 2p line (Fig. 8, curves a and b) are quite similar to those obtained for titanium carbide nitride [27], titanium nitride [28] or titanium oxynitride containing low amounts of oxygen [29]. Moreover, the binding energies obtained for Ti $2p_{3/2}$ contributions between 454.9 and 455.6 eV are also characteristic of these compounds. In zone I, there is few nitrogen and oxygen in the films (Fig. 1) and the C/Ti ratio is close to 1, therefore the growth of almost stoichiometric TiC containing small amounts of oxygen and nitrogen can be proposed.

For the highest (C + N + O)/Ti atomic ratios (zone II), the shape of the Ti 2p line (Fig. 8, curves d and e) can be identified as that characteristic of titanium dioxide, TiO_2, after bombardment [29] with

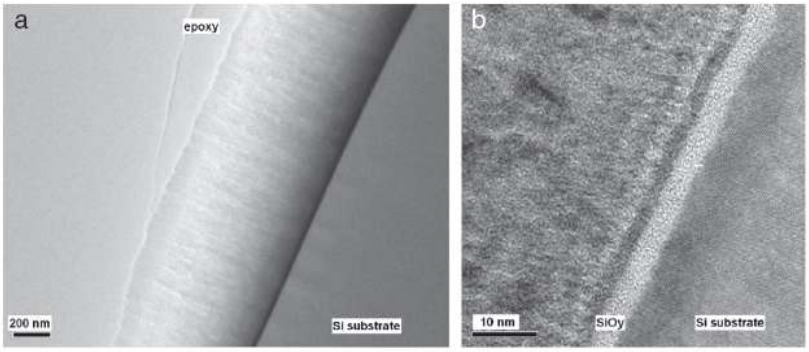

Fig. 4. TEM (a) and HRTEM (b) cross section image of the film deposited with $p_{O2+N2} = 0.4$ Pa.

the first one, 100–900 cm^{-1} range, shows acoustical and optical modes of titanium compounds, and the second one, 1100–1800 cm^{-1} range, displays C–C stretching modes. Other contributions, involving for example C–O vibrations, were not identified in this range, though a small component in the C 1s XPS line was associated to C–O bonds (see Section 3.2). No Raman bands were found in the 2000–2400 cm^{-1} range corresponding to C≡N stretching vibrations.

It is important to remember that in the case of compounds with the rock–salt structure, as TiC, TiN and TiO, no vibrational modes are active in Raman due to symmetry rules. Raman spectra of these compounds display large bands which are induced by disorder [20]. On the contrary, titanium dioxide crystallized in anatase, rutile or brookite phases, as well as other Ti sub-oxides such as Ti_2O_3, have several active Raman modes with frequencies in the 100–900 cm^{-1} range [15,17]. Moreover, crystallized titanium dioxide is a high Raman scatterer, which allows detecting very small amounts of this phase by Raman spectroscopy [21]. In the spectra of Fig. 6, no band can be associated to crystallised titanium dioxide or other Ti sub-oxide even for the highest gas mixture partial pressures.

For the lowest $O_2 + N_2$ partial pressures (zone I, $p_{O2+N2} \leq 0.09$ Pa), the spectra display a broad band at 620 cm^{-1} and a lower intensity band with two bumps at 277 and 360 cm^{-1}. This spectrum can be assigned to titanium carbide in agreement with XRD results. The increase of the $O_2 + N_2$ partial pressure (zone II) gives rise to an increasing broadening of the Raman bands, but no significant shift of these bands is observed. The broadening of the Raman bands is consistent with the increase of disorder in the f.c.c. structure due to the increasing amount of N and O within the films.

In the second spectral region of Fig. 6, the spectra display two bands centered at 1408 cm^{-1} and 1580 cm^{-1}, labeled D and G,

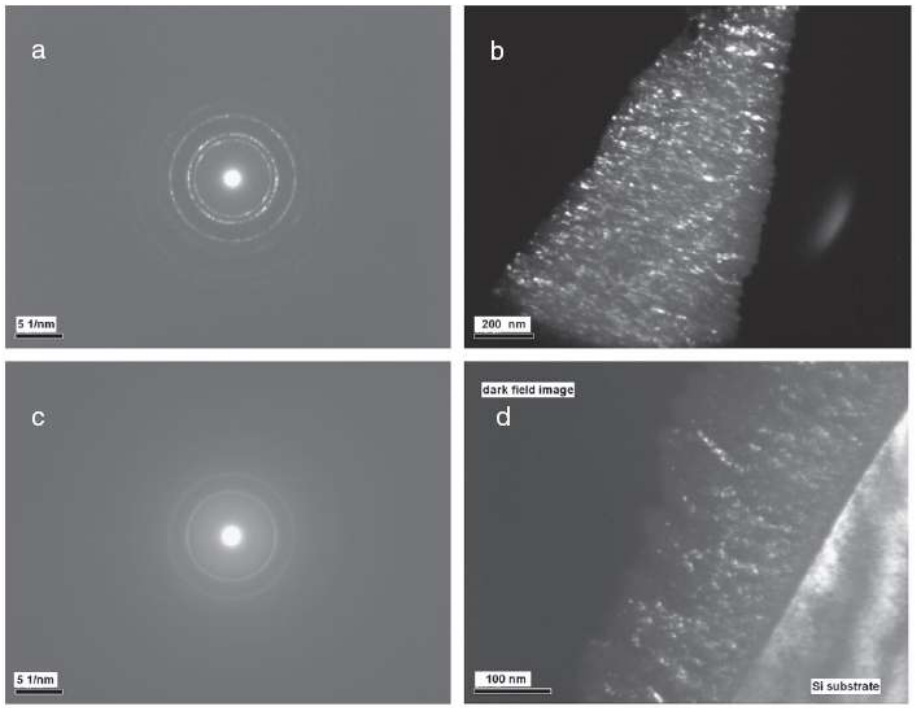

Fig. 5. Diffraction patterns (a,c) and dark field images (b,d) obtained for samples deposited with $p_{O2+N2} = 0.11$ Pa (a,b) and 0.40 Pa (c,d), respectively.

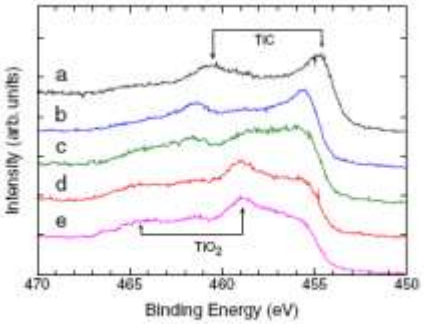

Fig. 8. XPS Ti 2p lines of titanium oxycarbonitride thin films deposited by reactive sputtering with different $O_2 + N_2$ partial pressures: from top to bottom $p_{O2+N2} = 0$ Pa (a); 0.09 Pa (b); 0.11 Pa (c); 0.22 Pa (d); and 0.40 Pa (e).

a maximum at 458.9 eV for the Ti $2p_{3/2}$ contribution. Nevertheless, similar spectra have also been reported in the case of titanium oxynitride films containing high amounts of oxygen (around 40 at. %), which give rise to the growth of amorphous titanium dioxide [29]. In zone II, the amount of oxygen increases continuously, while that of nitrogen is almost constant (around 30 at. %), and the (C + N + O)/Ti ratio is close to 4. These results suggest the growth of i) titanium dioxide containing nitrogen and carbon as impurities and/or ii) over-stoichiometric Ti(C,N,O) containing a very high amount of oxygen and nitrogen.

For the film obtained with a partial pressure of 0.11 Pa, the shape of the Ti 2p line (Fig. 8, curve c) is a combination of the Ti 2p lines characteristic of zones I and II.

The position and the shape of the N 1s line are always the same, whatever the atomic ratios revealed by the samples. One example is proposed in Fig. 9a for ($O_2 + N_2$) partial pressure around 0.11 Pa. This line is composed of two contributions: the main component at 397.1 eV is attributed to the titanium oxynitride phase [4,30,31], and the second one at 399.4 eV to C–N bonds [4,32].

Concerning the O 1s line, and similarly to what was observed for the N 1s line, the position and shape of the peaks are the same for all for the samples. Fig. 9b presents one example. Indeed, oxygen chemical environment is not different enough between phases like TiO_2 and Ti(N,O) to be distinguished in XPS. The second contribution at 532.9 eV is usually attributed to C–O bonds [33].

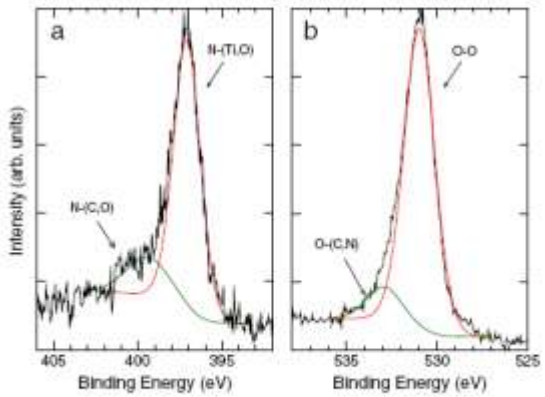

Fig. 9. XPS N 1s line (a) and O1s line (b) of titanium oxycarbonitride thin film deposited by reactive sputtering with $p_{O2+N2} = 0.11$ Pa.

Last, the most interesting information is given by the C 1s line, which is presented in Fig. 10 for two ($O_2 + N_2$) partial pressures, one in zone I (curve a in Fig. 10) and the second one in zone II (curve b in Fig. 10). The line is composed of at least three different contributions, the relative weight of each changing a lot between the two zones: the first contribution, located at 282.1 eV can be attributed to TiC [34]. The second component situated at 284.5 eV is commonly admitted to be the reference for C–C bonds of elementary carbon [35]. This position could also correspond to C–H bonds, but the presence of this kind of compounds seems unlikely after thirty minutes of bombardment. Then, a third component located at about 1.5 eV higher binding energies can be attributed to C–O bonds [36]. A small additional component can eventually be added at higher binding energies and attributed to multiple bonds between oxygen and carbon or to carbon–nitrogen bonds. As its relative intensity greatly depends on the way the C 1s line is modeled, only the sum of components 3 and 4 will be further considered and labeled C–(O,N) component.

It is clear by comparison of curves (a) and (b) in Fig. 10 that, when p_{O2+N2} increases (and thus (C + N + O)/Ti increases), the contribution corresponding to C–Ti bonds decreases while the one of C–C bonds increases. In order to get further information, the evolution of the relative areas of C–Ti, C–C and C–(O,N) components in the C 1s line are presented in Fig. 11 as a function of the $O_2 + N_2$ partial pressure. The relative areas remain roughly constant for low and high p_{O2+N2} while C–Ti and C–C contributions vary in opposite ways, the first one decreasing and the second one increasing for intermediate p_{O2+N2} values. Moreover, the evolution of the sum of the third and fourth component is identical to the C–C component one.

As a first assessment of the overall results of the XPS analysis, it can be proposed that there are different phases growing in the films of zones I and II. When the gas mixture partial pressure is low (zone I), the main phase is almost stoichiometric TiC containing small amounts of oxygen and nitrogen. In zone II, the high affinity of oxygen towards titanium pushes carbon away from the titanium neighboring. Thus, a phase containing C–C bonds appears, with an amount that increases with the increasing of p_{O2+N2}. Other phase(s) contains titanium, which is mainly bonded to oxygen, as in titanium dioxide, and a high amount of nitrogen. Thus, the growth of nitrogen-enriched titanium dioxide and/or over-stoichiometric Ti(N,O) containing a high amount of oxygen can be proposed in zone II, in addition to a phase with C–C bonds. The inversion of the dominating phases in the films occurs for p_{O2+N2} in the 0.11–0.15 Pa range.

4. Discussion

The atomic ratios C/Ti, N/Ti, O/Ti and C + N + O/Ti displayed in Fig. 1 allow checking some possible correlation between elemental composition and the compounds that may be formed. In zone I, the

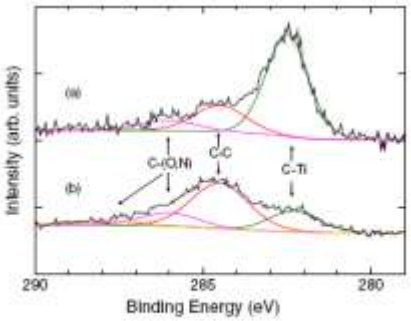

Fig. 10. XPS C 1s line of titanium oxycarbonitride thin film deposited by reactive sputtering with $p_{O2+N2} = 0.09$ Pa (a) and 0.22 Pa (b).

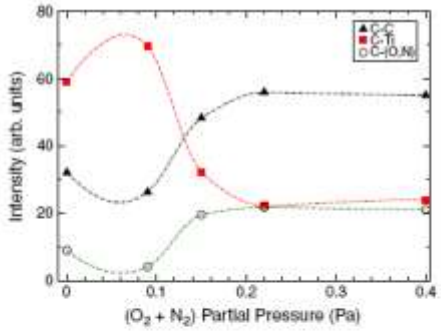

Fig. 11. Evolution of the relative contributions of C–Ti, C–C and C–(O,N) components in the C 1s line as a function of the $O_2 + N_2$ partial pressure.

atomic ratio between titanium and the other elements (C + N + O/Ti) ranges from 0.8 to 2.6, with a dominant contribution of carbon which is due to the low $O_2 + N_2$ partial pressure compared to the constant injection of acetylene in the deposition chamber. Moreover, the individual ratios, C/Ti, O/Ti and N/Ti are below 1, which suggests an association of titanium with one or several of the three non metals to form a compound of the type $Ti–(C,N,O)_x$ with $0.8<x<2.6$, where C and/or N and/or O may be simultaneously bonded to titanium. At these low flow rates, the films are nearly stoichiometric and thus most of the sputtered atoms as well as the reactive ones present in the plasma are included in the growing film. This regime can be considered as being in an approximately kinetics-driven mode and thus the evolution of the film composition strongly depends on the gas mixture partial pressure. Interesting to note is that the standard enthalpies of formation of TiC, TiN, TiO and TiO_2 compounds are respectively, −184, −338, −520 and −942 $kJ.mol^{-1}$. Therefore the higher affinity of titanium towards oxygen induces much higher oxygen content in the film (Fig. 1a) than the one expected from the gas mixture composition (85% of nitrogen, 15% of oxygen).

In zone II, the ratio (C + N + O)/Ti "jumps" to relatively high values, close to 4 (3.3 to 4.4), as seen in Fig. 1b. These high values correspond to a quite different behaviour from that of zone I. There are now probably not enough free titanium atoms to establish bonds with the three other elements. Moreover, by a quick look at the evolution of both elemental concentrations and atomic ratios in this zone, the film composition seems to depend less directly on the mixture partial pressure, but more on the thermodynamic constraints. In fact, as the reactive gas mixture increases, the oxygen content and the O/Ti ratio are both increasing (Fig. 1a), but the nitrogen content (as well as the N/Ti ratio) is approximately constant, in spite of the much higher content of this element in the gas mixture (85% of nitrogen, 15% of oxygen). This evolution indicates that the higher affinity of titanium towards oxygen plays the dominant role and favours the possibility to form TiO_2-type compounds, as suggested by the thermodynamic data. Nevertheless, the O/Ti ratio, though increasing in this zone, ranges only between 0.65 and 1.20. Moreover, both N/Ti and C/Ti ratios are relatively high (roughly above 1), which implies that these two elements might be also playing an important role in the types of bonds developed by titanium. Finally, the C/Ti atomic ratio decreases from about 1.85 to 0.75, which suggests a change in the bonds formed by carbon in the films of zone II, as it was shown by XPS results.

Now, the aim is to correlate the structural and chemical characteristics of the films with the corresponding optical properties (Fig. 2). In zone I, the films are dark grey and very slightly brownish. The reflectance increases continuously to higher wavelengths in the visible range, which is characteristic of a metallic material. In zone II, the reflectance is almost constant around 15% in the visible range and the colour CIElab coordinates are those corresponding to black for a human observer.

Besides the amorphisation of the films with the increase of the gas mixture partial pressure, shown by XRD, TEM and Raman, two main results give new information for explaining the change of the optical properties: i) the high increase of the carbon Raman modes in zone II which reveals the growth of amorphous carbon within the films of zone II, ii) the change of both the Ti 2p and the C1s XPS line shapes. The Ti 2p line reveals the modification of the local environment of Ti atoms: mainly Ti–C bonds in zone I, whereas Ti–O bonds dominate in zone II. The C 1 s line shows that the number of carbon atoms bonded to Ti is low in zone II, whereas the number of carbon–carbon bonds increases. Taking into account these results, the change in the optical properties of the films can be explained as follows: in zone I the films are polycrystalline TiC containing small amounts of oxygen, whereas in zone II two phases are formed within the films: amorphous $Ti_x(O,N)_y$ with few carbon atoms inside and amorphous carbon. The films are no more metallic-like and the colour becomes black due to the presence of amorphous carbon.

The changes observed in the films when increasing the gas mixture partial pressure above 0.15 Pa (zone II) suggest that the mechanisms involved in the deposition process can also be modified. The fact that the ratio (N + O + C)/Ti increases rapidly above 1 (in zone II) shows the transition from a situation where almost all arriving species are added to the growing film (first zone), to a zone where the excess of (N + O + C)/Ti is most likely inducing some preferential reactions of Ti, according to the reactivity of each reactive gas. In zone II, the films lose their long range order, which may result from the joined effects of both low surface diffusion of the particles impinging on the substrate or the growing film (the depositions were made at only 473 K and no bias was used), and the significant over-stoichiometric condition of the films (Ti is only around 20 at. % within the high partial pressures zone).

5. Conclusions

It has been shown that the structure and the chemical bonds in Ti–C–N–O films, grown by reactive sputtering, can be modified through the variation of the $O_2 + N_2$ gas mixture partial in the range 0 to 0.4 Pa, keeping constant the acetylene partial pressure at 0.25 Pa.

For the lowest $O_2 + N_2$ gas mixture partial pressures, the films are polycrystalline, with a structure similar to that of TiC, becoming amorphous with the increase of the $O_2 + N_2$ gas mixture partial pressure above 0.15 Pa. Significant changes were also observed in the optical properties and the colour of the films.

XPS results showed the change of both the Ti 2p and the C 1s line shapes for $O_2 + N_2$ partial pressures higher than 0.15 Pa. In particular, the relative contribution of C–Ti bonds to the C 1s line decreased, while that of C–C bonds increased with the increase $O_2 + N_2$ partial pressure. The higher affinity of titanium towards oxygen and nitrogen than to carbon explains these changes in the nature of the chemical bonds developed by carbon and titanium.

In the corresponding Raman spectra, the significant increase in the intensity of the carbon Raman modes, for $O_2 + N_2$ partial pressure higher than 0.15 Pa, is consistent with the growth of amorphous carbon, coexisting with titanium oxynitride.

The evolution of the optical properties and the colour of the films from metallic grey to deep black can be explained by the growth of a nanocomposite structure, where amorphous carbon coexists with poorly crystallized titanium oxynitride.

Acknowledgements

This research is partially sponsored by FEDER funds through the program COMPETE - Programa Operacional Factores de Competitividade

and by national funds through FCT - Fundação para a Ciência e a Tecnologia, under the project PTDC/CTM/69362/2006.

The authors thank also the "Fundação para a Ciência e Tecnologia" of Portugal for the post-doctorate grant SFRH/BPD/27114/2006. The authors also thank CRUP (Acção Integrada Luso-francesa N° F-2307) and the GRICES/CNRS collaboration (Proc. 4.1.1 França) for their financial support.

References

[1] D.A. Glocker, S.I. Shah, Handbook of Thin Film Process Technology, vol. 2, IOP Publishing, Bristol and Philadelphia, 1995.
[2] H. Randhawa, Surf. Coat. Technol. 36 (1988) 829.
[3] A.E. Kaloyeros, E. Eisenbraun, Annu. Rev. Mater. Sci. 30 (2000) 363.
[4] J.C.F. Rodríguez-Reyes, C. Ni, H.P. Bui, T.P. Beebe Jr., A.V. Teplyakov, Chem. Mater. 21 (2009) 5163.
[5] T. Zehnder, J. Patscheider, Surf. Coat. Technol. 133–134 (2000) 138.
[6] K. Narasimhan, S. Prasad Boppana, D.G. Bhat, Wear 188 (1995) 123.
[7] J.W. Elam, M. Schuisky, J.D. Ferguson, S.M. George, Thin Solid Films 436 (2003).
[8] J.Y. Yun, M.Y. Park, S.W. Rhee, J. Electrochem. Soc. 145 (1998) 2453.
[9] F. Fabreguette, L. Imhoff, M. Maglione, B. Domenichini, M.C. Marco de Lucas, P. Sibillot, S. Bourgeois, M. Sacilotti, Chem. Vapor Depos. 6 (2000) 109.
[10] A. Rizzo, M.A. Signore, L. Tapfer, E. Piscopiello, A. Cappello, E. Bemporad, M. Sebastiani, J. Phys. D: Appl. Phys. 42 (2009) 115406.
[11] A. Stanishevsky, R. Lappalainen, Surf. Coat. Technol. 123 (2000) 101.
[12] J.R. Sobiecki, P. Mankowski, T. Wierzchon, Vacuum 68 (2003) 105.
[13] J.H. Hsieh, W. Wu, C. Li, C.H. Yu, B.H. Tan, Surf. Coat. Technol. 163–164 (2003) 233.
[14] J.H. Hsieh, C. Li, W. Wu, A.L.K. Tan, J. Mater. Process. Technol. 140 (2003) 662.
[15] L. Lavisse, P. Berger, M. Cirisan, J.M. Jouvard, S. Bourgeois, M.C. Marco de Lucas, J. Phys. D: Appl. Phys. 42 (2009) 245303.
[16] J. Alami, K. Sarakinos, F. Uslu, C. Klever, J. Dukwen, M. Wuttig, J. Phys. D: Appl. Phys. 42 (2009) 115204.
[17] S. Bouknuh, R. Bensaha, S. Bourgeois, E. Finot, M.C. Marco de Lucas, Thin Solid Films 516 (2008) 6353.
[18] N. Martin, O. Banakh, A.M.E. Santo, S. Springer, R. Sanjinès, J. Takadoum, F. Lévy, Appl. Surf. Sci. 185 (2001) 123.
[19] J.M. Chappé, F. Vaz, L. Cunha, C. Moura, M.C. Marco de Lucas, L. Imhoff, S. Bourgeois, J.F. Pierson, Surf. Coat. Technol. 203 (2008) 804.
[20] W. Spengler, N.A. Christensen, G. Müller-Vogt, Phys. Rev. B 17 (1978) 1095.
[21] C. Pighini, D. Aymes, N. Millot, L. Saviot, J. Nanopart. Res. 9 (2007) 309.
[22] A.C. Ferrari, J. Robertson, Phil. Trans. R. Soc. Lond. A 362 (2004) 2477.
[23] A.C. Ferrari, J. Robertson, Phys. Rev. B 61 (2000) 14095.
[24] A.C. Ferrari, J. Robertson, Phys. Rev. B 64 (2001) 075414.
[25] J.C. Sanchéz-Lopez, D. Martinez-Martinez, C. Lopez-Cartes, A. Fernandez, Surf. Coat. Technol. 202 (2008) 4011.
[26] L. Zhang, R.V. Kola, Mater. Chem. Phys. 57 (1998) 23.
[27] I.N. Mihailescu, N. Chitica, V.S. Teodorescu, M. Popescu, M.L. de Giorgi, A. Luches, A. Perrone, Ch. Boulmer-Leborgne, J. Hermann, B. Dubreuil, S. Udrea, A. Barbonica, I. Iova, J. Appl. Phys. 75 (1994) 5286.
[28] A. Toth, I. Bertoti, M. Mohai, M. Revesz, Acta Chim. Hung. - Model. Chem. 130 (1993) 837.
[29] J. Guillot, F. Fabreguette, L. Imhoff, O. Heintz, M.C. Marco de Lucas, M. Sacilotti, B. Domenichini, S. Bourgeois, Appl. Surf. Sci. 177 (2001) 268.
[30] J. Guillot, A. Jouaiti, L. Imhoff, B. Domenichini, O. Heintz, S. Zerkout, A. Mosser, S. Bourgeois, Surf. Interface Anal. 34 (2002) 577.
[31] J. Tong, N. Magtoto, J. Kelber, Appl. Surf. Sci. 220 (2003) 203.
[32] M. Jelinek, J. Zemek, M. Trchova, V. Vorlicek, J. Lancok, R. Tomov, M. Simeckova, Thin Solid Films 366 (2000) 69.
[33] D. Rats, L. Vandenbulcke, R. Herbin, R. Benoit, R. Erre, V. Serin, J. Sevely, Thin Solid Films 270 (1995) 177.
[34] H.J.P. Johansson, K.L. Hakansson, L.I. Johansson, Phys. Rev. B 48 (1993) 14520.
[35] A. Tressaud, E. Papirer, F. Moguet, G. Nanse, P. Fioux, Carbon 35 (1997) 175.
[36] A. Brevet, P.M. Petesté, L. Imhoff, M.C. Marco de Lucas, S. Bourgeois, J. Cryst. Growth 275 (2005) e1263.